ELSEVIER

NeuroImage

www.elsevier.com/locate/ynimg
NeuroImage 31 (2006) 1549 – 1559

Technical Note

Finger motion sensors for fMRI motor studies

Judith D. Schaechter,[a,b,*] Christopher Stokes,[c] Brendan D. Connell,[a,b] Katherine Perdue,[a,b] and Giorgio Bonmassar[a,b]

[a]*MGH/MIT/HMS Athinoula A. Martinos Center for Biomedical Imaging, 13th Street, Building 149, Room 2301, Charlestown, MA 02129, USA*
[b]*Department of Radiology, Harvard Medical School, Boston, MA 02115, USA*
[c]*Rowland Institute at Harvard, Cambridge, MA 02142, USA*

Received 24 October 2005; revised 12 January 2006; accepted 16 February 2006
Available online 19 April 2006

The kinematics of motor task performance affect brain activity. However, few functional magnetic resonance imaging (fMRI) motor studies have accounted for on-line kinematics because there are currently few MRI-compatible devices to record motor performance. We built a device based on Micro-Electro-Mechanical System (MEMS) gyroscopes that measures the angular velocity of one segment of each of the 10 fingers while a subject performs a finger motor task during fMRI. Finger position, acceleration, and jerk were computed from the angular velocity measurements. The signal-to-noise ratio (SNR) of the MEMS sensors (range: 27.10–34.36 dB) allowed for clear detection of velocity of finger motion during fMRI motor task performance, and showed good stability over time. We demonstrate that use of the MEMS-based device, while negligibly increasing radiofrequency (RF) noise in the scanning environment, did not cause MR image artifacts nor alter fMRI statistical activation maps. Further, we show that signal from the MEMS sensors was not affected by the high static magnetic field (3 T). Increasing the RF power transmitted during fMRI by using a body coil, as compared to a head coil, decreased the sensor's SNR from 30.7 to 24.2 dB, though this loss in SNR did not interfere with the ability to measure velocity of finger motion. We demonstrate the utility of the MEMS-based device in fMRI motor studies through two experiments that examined the relationship between finger movement kinematics and fMRI activation in the healthy and injured brain. On-line acquisition of motor performance during fMRI, through the use of the MEMS-based device, promises to allow for a more detailed understanding of the relationship between movement kinematics and activation in the healthy and injured brain.

Keywords: Device; MEMS; Gyroscope; Movement; Kinematics

Introduction

A major application of functional magnetic resonance imaging (fMRI) is the study of brain mechanisms controlling voluntary movement in humans, and reorganization of this system in response to injury, such as stroke and Parkinson's disease (for review, see Rowe and Frackowiak, 1999). The kinematics of motor performance have been shown to affect brain activation (Cramer et al., 2002; Ehrsson et al., 2001; Rao et al., 1996; Waldvogel et al., 1999; Wexler et al., 1997). However, relatively few fMRI motor studies have recorded performance on-line because the signal from a motion sensor can be grossly contaminated by induced noise from the scanning environment, and because presence of a sensor during fMRI can result in image artifacts. Exceptions have been the use of a non-ferromagnetic (Cramer et al., 2002; Ehrsson et al., 2001) or hydraulic (Liu et al., 2000) force transducer to measure handgrip force, and an accelerometer (Morgen et al., 2004) and electrogoniometer (Carey et al., 2002) to monitor movement of a single finger during fMRI. In contrast, most fMRI motor studies resort to visual monitoring. While visual monitoring during the fMRI experiment allows for crude assessment of whether the subject performed the motor task correctly, it lacks the ability to quantify the kinematics of motor performance. Quantitative assessment of on-line motor performance would be expected to provide a more detailed understanding of the relationship between kinematics of motor performance and activation in the healthy and injured brain.

We built a device for measuring angular velocity of one segment of each of the 10 digits during fMRI using Micro-Electro-Mechanical System (MEMS) gyroscopes. We demonstrate that the scanning environment does not interfere with the ability to accurately record the finger motion measurements using the MEMS-based device, and, reciprocally, its use does not cause image artifacts or alter fMRI statistical activation maps. Further, we provide two examples of the utility of the MEMS-based device in fMRI motor studies.

* Corresponding author. MGH/MIT/HMS Athinoula A. Martinos Center for Biomedical Imaging, 13th Street, Building 149, Room 2301, Charlestown, MA 02129, USA. Fax: +1 617 726 7422.
E-mail address: judith@nmr.mgh.harvard.edu (J.D. Schaechter).
Available online on ScienceDirect (www.sciencedirect.com).

1053-8119/$ - see front matter © 2006 Elsevier Inc. All rights reserved.
doi:10.1016/j.neuroimage.2006.02.029

Materials and methods

Finger motion sensing device

Fig. 1 is a schematic of the MEMS-based device with its component parts. Single chip yaw rate (±150°/s) gyroscopes (Analog Devices, Norwood, Massachusetts, Part # ADXRS150) were used, with each chip being 7 mm × 7 mm × 3 mm in size, and <0.5 g in weight (Geen et al., 2002). Each MEMS sensor was mounted on a circuit board (10 mm × 8 mm × 0.5 mm; 2 layers; thickness = 0.031 in; dielectric = FR-4; hole size minimum/maximum = 0.015/0.030 in.; trace thickness minimum = 0.010 in.). The external components were chosen for bandwidth set to −3 dB roll-off at 80 Hz, and the dynamic measurement range set to ± 300°/s (using an external resistor of 180 kΩ), providing a sensitivity of 6.3 mV/°/s. Power (5 V, 6 mA) was supplied to each sensor via a filtered connector by a laptop computer's (Toshiba PC2100) analog-to-digital card (Measurement Computing, Middleboro, MA, PC-CARD-DAS16/16).

Fig. 2 shows the finger motion sensors positioned on a subject's hand. Each sensor/circuit board unit was epoxy-mounted to a remodeled plastic guitar pick (approximately 15 mm × 15 mm × 1 mm) such that when secured (by double-sided tape) to the dorsal, proximal segment of a digit, the rate-sensing *z* axis was perpendicular to the long axis of the digit. This positioning allowed detection of angular velocity (hereafter referred to as velocity) during flexion and extension at the metacarpophalangeal joint of the digit.

Extending from each sensor/circuit board unit was 22 cm of shielded and jacketed cable (Cooner Wire, Part #AS 999-32-3SJ). The cable from each of the five sensor/circuit board units from one hand was connected to a circuit board (32 mm × 40 mm × 1.5 mm; 2 layers; thickness = 0.060 in.; dielectric = FR-4; hole size minimum/maximum = 0.50/0.85 in.; trace thickness minimum/maximum = 0.010/0.20 in). Low eddy current ground-planes were etched into the circuit board in a diagonal grid pattern (line width/spacing = 25/25 mil) that was 15 mil from the signal traces. This circuit board was secured to the wrist by a cloth/velcro watchband that included a 15-pin connector for signal transmission and power supply, and a male end Hirose 3560-10S 10-pin surface mount receptacle. Inclusion of the surface mount receptacle provided an easy means of securing the sensors onto a subject's hand without the encumbrance of attached cabling. Twenty-five feet of shielded and jacketed cable (Cooner Wire, Chatsworth, CA, Part #AS 148 REV1) extended from the female end of a Hirose 3530 10-pin connector. At the end of this cable was a 15-pin connector that attached to a connector permanently installed in a shielded, wall-mounted penetration panel in the MRI scanning room. Available cabling was used to carry signal outside the MRI scanning room to a junction box that included a common-mode transformer to remove ground loop and power line noise. A ribbon cable connected the junction box to a 16-channel, 100 kHz, 16-bit analog-to-digital card (Measurement Computing, PC-CARD-DAS16/16) that was loaded into the laptop computer. Data acquisition software was written in Visual C++ (Microsoft, v6.0) and used Universal Library (Measurement Computing, v5.43) to interface with the analog-to-digital card. Prior to scanning each subject, we verified the response of each sensor to motion using the software Instacal (Measurement Computing).

The design of the device prevented contact between all conductive components and a subject, and thus the possibility of electric shock was highly improbable. Nonetheless, to prevent accidental electrical shock in the case of a component failure that could lead to creation of a conductive path (Reilly, 1998), we took the added precaution during MRI of powering the laptop computer by battery.

Upon building the finger motion sensing device, we noted that the sensors were slightly magnetic. Therefore, we tested the sensors' translational attraction using the deflection angle test as recommended by the American Society for Testing and Materials for evaluating the safety of devices for use in MRI (Shellock, 2002). According to this procedure, the deflection angle of the device is measured at the point of the highest spatial gradient of the MR system. If the deflection angle from vertical is less than 45°, the device passes the translational attraction test. We tested the translational attraction of the sensors along a path from approximately 0 T to 3 T (the magnet's isocenter). Nowhere along this path did the device deflect greater than 45° from vertical. This result indicates that the sensors' translational attraction did not pose a safety risk to humans under the MR conditions applied in this study.

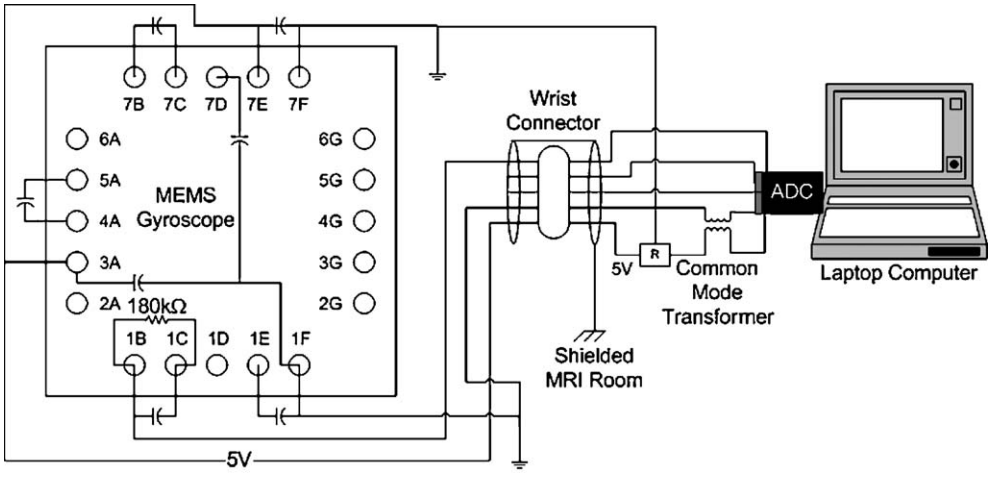

Fig. 1. Schematic of the MEMS-based device for sensing finger motion. Each MEMS gyroscope (1 of 10 depicted) was connected to a wrist connector, and then to a transformer. The transformer was connected to an analog-to-digital converter that was loaded into a laptop computer. The parts are not drawn to scale. R = regulator; ADC = analog-to-digital converter.

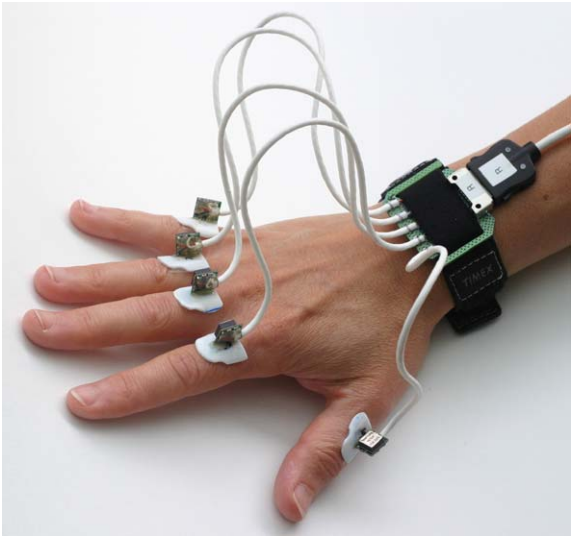

Fig. 2. The finger motion sensors secured on the hand of a subject.

Common MRI methods and analyses

A whole-body 3 T Siemens Trio scanning system was used for all experiments. Either a transmitter/receiver Bruker circular polarization head coil or an eight-channel receiver MRI Devices Corporation head coil was used for brain imaging experiments described below. Unless stated otherwise, subjects were positioned supine with the motion sensors secured to the hands, and the hands resting on the thighs. For the typical-sized adult lying in this position, the sensors were at the level of the outer edge of the scanner bore, and in this position, there was no perceivable magnetic pull on the sensors.

Structural imaging was conducted using a T1-weighted MPRAGE sequence (repetition time (TR) = 7 ms; echo time (TE) = 3 ms; flip angle (α) = 7°; field-of-view (FOV) = 256 mm × 256 mm; matrix size = 192 × 256; effective slice thickness = 1.33 mm). Blood oxygenation level-dependent (BOLD) functional imaging was conducted using a T2*-weighted gradient-echo, echo planar imaging sequence (TR = 1500; TE = 30 ms; α = 90°; FOV = 200 mm × 200 mm; matrix size = 64 × 64; slice thickness = 5 mm; interslice gap = 1 mm; number of slices = 23) equipped with real-time correction for head motion (Thesen et al., 2000). One of three finger motor tasks was performed during each fMRI experiment described below. Each finger motor task was cued visually via a projection system.

MRI data were analyzed using FreeSurfer (http://surfer.nmr.mgh.harvard.edu), Analysis of Functional NeuroImages (AFNI), and Surface Mapping with AFNI (SUMA) (http://afni.nimh.nih.gov) software. Each subject's T1-weighted structural images were used to generate a model of the cortical surface (Dale et al., 1999). Prior to statistical analysis, the functional images were motion-corrected, intensity-normalized, spatially smoothed using a three-dimensional Gaussian kernel (full-width at half-maximum (FWHM) = 3 mm), and aligned with the structural data. The volumetric functional data were mapped to the cortical surface model. The surface-based functional data were spatially smoothed using a two-dimensional Gaussian kernel (FWHM = 3 mm).

Common on-line finger motion sensing methods and analyses

Signal from the MEMS-based device was acquired at 1000 Hz. For experiments in which finger motion data were acquired during fMRI, we also collected calibration data (5 s rest; 18 s through maximal range of digit flexion and extension). This calibration data were used to scale the sensor data acquired during the experiment relative to each subject's full range of digit motion.

Unless otherwise noted, velocity time-series data were baseline-corrected based on the average motion-free signal of the first rest epoch. The data were then inverted to have finger extension relative to the rest position reflected in positive voltages, and finger flexion relative to the rest position reflected in negative voltages. Occasionally, we found that finger velocity during a movement epoch exceeded the measurement range of the sensors, resulting in a saturated signal. We estimated the signal during a saturated period by extrapolating from a cubic polynomial spline function fit to the neighboring data.

Several computations based on the velocity time-series were made in MATLAB (The Mathworks, v6.0 R12), depending on experimental needs. These computations included the duration, frequency, and speed of finger motion during movement epochs. Finger acceleration and jerk time-series were computed from the velocity time-series by applying a low-pass filter (9th order digital Butterworth, cutoff frequency = 20 Hz), and then taking the first and second derivative of the filtered time-series, respectively. The derivatives were calculated using the MATLAB 'diff' function which computes the difference between adjacent values in the time-series as: $A = \mathrm{diff}(V) \cdot F_S$; $J = \mathrm{diff}(\mathrm{diff}(V)) \cdot F_S^2$; where V = velocity, A = acceleration, J = jerk, and F_S = the sampling frequency. Finger position time-series were computed by integrating the velocity time-series over time. Drift in the baseline position over time was corrected by calculating the average signal 11.25 to 2 s before each movement epoch and 2 to 11.25 s after each movement epoch, and then linearly interpolating the baseline during each movement epoch. This linear result was subtracted from the position values computed during each movement epoch. Each finger's position time-series was scaled relative to maximum amplitude, where 0% = full flexion and 100% = full extension.

Characterizing the MEMS sensor signal (Experiment 1)

Experiment 1 characterized the signal from the MEMS-based device acquired during fMRI. For this experiment, two adults (1 male, age 46 years; 1 female, age 62 years) fitted with the MEMS sensors performed a motor task while fMRI was conducted using the transmitter/receiver head coil. The motor task was in-phase flexion and extension of the five digits (henceforth called five-digit motor task) of the right hand at 0.25 Hz (one flexion/extension cycle per 4 s). Performance of the five-digit motor task (22.5 s × 5) alternated with the fingers resting (22.5 s × 6) in a block-design paradigm. The velocity time-series of the sensor signal from all digits of the right hand of each subject were analyzed to evaluate the following characteristics: (1) baseline noise range (N), taken as the MEMS sensor signal during rest epochs, with $N = V_{max}(R) - V_{min}(R)$, where V = volts and R = rest epoch of the velocity time-series, then averaged over the six rest epochs; (2) signal range (S), taken as the dynamic range of the MEMS sensor signal, with $S = V_{max} - V_{min}$; and (3) SNR as $20 \log_{10}(S / N)$. Short-term and long-term stability of the MEMS sensor signal was characterized by comparing: (1) average baseline noise amplitude (prior to baseline-

correction) and baseline noise range during the first and last rest epochs of the velocity time-series collected during a single fMRI run; and (2) range of baseline noise, signal, and SNR of velocity time-series collected during an fMRI run and another run collected 2 weeks later.

Effect of MRI on the MEMS sensor signal (Experiments 2 and 3)

There are three potential sources of contamination of the MEMS sensor signal due to MRI: the static magnetic field, the gradient magnetic field produced by time-varying gradient currents, and the radiofrequency (RF) field. During fMRI of a typical-sized adult human subject, the position of the MEMS sensors when mounted on the fingers is at least 70 cm from the head. At this distance from the magnet's isocenter, the time-varying gradient magnetic field is approximately zero. Therefore, we tested whether the static magnetic field and RF field, but not the time-varying gradient magnetic field, affected the MEMS sensor signal.

Experiment 2

This experiment tested whether the high static magnetic field corrupted the MEMS sensor signal collected during finger motion. For this test, a subject (female, age 45 years) fitted with the MEMS sensors performed the five-digit motor task at high static magnetic field (3 T) and again at low static magnetic field (44 G, measured with Gaussmeter Model 421 and probe Model MMA-1808-WL, Lake Shore Cryotronics Inc.). The sensors were exposed to the high static magnetic field by having the subject lie prone on the scanner bed with the hands extended into the scanner bore to the imaging FOV. The sensors were exposed to the low static magnetic field by having the subject's hands positioned at the end of the scanner bed that had been maximally withdrawn from the bore. No scanning sequence was run during this experiment. The velocity time-series of the sensor signal collected at high and low static magnetic fields were cropped to remove signal acquired during the rest epochs, leaving the velocity time-series collected during the movement epochs. The correlation coefficient (r; range 0 to ±1) between the two movement velocity time-series from a representative finger (middle finger of the right hand) was determined using the MATLAB 'corrcoef' function. The MATLAB function transformed the r value into a t statistic, from which its P value was computed. Alpha was set to 0.01.

Experiment 3

We examined the effect of the RF field during fMRI on the MEMS sensor signal by comparing the sensor's SNR when imaging was conducted using the transmitter/receiver head coil versus the eight-channel receiver head coil. The transmitted RF power from the body coil when using the eight-channel receiver head coil is 2.86 times greater than that from the head coil, which could increase noise in the MEMS recording. For this test, the MEMS sensors were secured to the fingers of a subject (male, age 23 years). The subject performed the five-digit motor task with the right hand while fMRI was conducted using the transmitter/receiver head coil, and again using the transmitter body coil with the eight-channel receiver head coil. The SNR (20 $\log_{10}(S/N)$) of the sensor signal from a representative finger (middle finger of the right hand) was computed under the two conditions. The baseline noise range ($N = V_{max}(R) - V_{min}(R)$) was computed for each rest epoch of the velocity time-series, then averaged over the six rest epochs. The signal range was taken as the dynamic range ($S = V_{max} - V_{min}$) of the MEMS sensors.

Effect of MEMS-based device on RF noise and fMR images (Experiments 4 and 5)

We tested if using the MEMS-based device increased RF noise in the ambient scanning environment (Experiment 4) or produced fMR image artifacts (Experiment 5).

Experiment 4

RF noise imaging was conducted to test whether the MEMS-based device increased RF noise in the ambient scanning environment. A subject (male, age 33 years) was positioned supine in the scanner bore with the transmitter/receiver head coil. A Siemens quality testing sequence (TR = 1400 ms; TE = 1 ms; FOV = 100 mm × 100 mm; matrix size 256 × 256) collected 50 images over the bandwidth of 122.95 to 123.45 MHz (centered about 123.2 MHz—the resonance frequency of water in the scanner) by shifting the center frequency of each image by 10 kHz. Each of the 50 images covered a 10 kHz spectrum in 39 Hz increments. The sequence was run four times—twice with the subject performing the five-digit motor task with the right hand while finger motion data were collected using the MEMS-based device, and twice with the subject performing the same motor task yet without the sensors present.

To evaluate whether use of the MEMS-based device introduced frequency-specific increases in noise, each RF noise image was visually inspected for artifacts. The RF noise sequence itself does not produce any RF signal or time-varying gradient magnetic fields. Therefore, an RF noise image with no signal contamination would appear as pure white noise. An artifact in an RF noise image would appear as a hyper-intense line in the phase-encoding direction. This method, albeit subjective, is considered a sensitive means of evaluating RF noise images for frequency-specific artifacts (personal communication, Franz Hebrank, Ph.D.). To evaluate for overall differences in RF noise under the two conditions, the following computations were performed. Signal (in arbitrary units) in each of the 50 images was averaged over the phase-encoding direction to obtain a vector of 12,800 samples reflecting signal across the 122.95 to 123.45 MHz spectrum. Vectors from replicate runs of each condition were averaged. Finally, a paired, two-tailed Student's t test was performed to test for differences between the two average vectors, with alpha set to 0.01. We estimated the magnitude of change (in percent) in RF noise due to use of the MEMS-based device in the MR scanner by computing the mean difference (sensors present-sensors absent) between the two average signals, dividing by the average signal when the sensors were absent, then multiplying by 100.

Experiment 5

We tested whether using the MEMS-based device during fMRI produced image artifacts or altered the statistical activation map. Two subjects (males, age 23 and 43 years) were positioned in the scanner with the eight-channel receiver head coil. Functional images were collected (number of acquisitions/slice = 165) while the subject repetitively flexed and extended the second digit (henceforth called D2 motor task) of the right hand at 0.5 Hz (one flexion/extension cycle per 2 s). Performance of the D2 motor task (22.5 s × 5) alternated with all fingers resting (22.5 s × 6) in a

block-design paradigm. Six sets of functional images were collected during which the MEMS sensors were alternately secured to the subject's hand, and removed from the subject's hand and placed outside the scanner's magnetic field.

Differences in the hemodynamic response to the subject's finger motion when the MEMS sensors were present as compared to when they were absent were computed across the cortical surface using a fixed-effects model. The statistical procedure used a general linear model that included a baseline linear drift term and motion-correction parameters as nuisance regressors. The canonical stimulus input function was a gamma function (delta = 2.25 s, tau = 1.25 s) (Dale and Buckner, 1999) convolved with a boxcar function. Resultant statistical activation maps were corrected to a false discovery rate (Genovese et al., 2002) of 1%. A second analysis compared the BOLD activation response in two regions-of-interest when the MEMS sensors were present versus absent. The regions-of-interest were the precentral gyrus (PRG) and postcentral gyrus (POG) within the hand region of the primary sensorimotor cortex. The hand area of the primary sensorimotor cortex was identified on the cortical surface as the first posterior convexity of the central sulcus lateral to the midline (Moore et al., 2000). Activation responses under the two conditions were compared for: (1) location of the most significantly activated vertex on the cortical surface, and the corresponding Talaraich coordinates; (2) spatial extent of the cluster of vertices contiguous with most significantly activated vertex; and (3) average magnitude of the BOLD activation response across all vertices of the cluster.

Application of the MEMS-based device in fMRI motor studies (Experiments 6 and 7)

We examined the utility of the MEMS-based device in fMRI motor studies in two experiments.

Experiment 6

We tested for brain areas with activity that was linearly dependent on the speed of finger movement. Two subjects (males, age 28 and 43 years) were positioned in the scanner with the eight-channel receiver head coil and MEMS sensors on the fingers. Two sets of functional images were collected (number of acquisitions/slice = 214) while the subject alternated between performing the D2 motor task (30 s × 6) with the right hand and resting (20 s × 7) in a block-design paradigm. During movement epochs, the subject was cued to perform the task over varying speeds in response to viewing a number ranging from 1 to 10, with 10 cueing for maximum speed. The number presented during movement epochs changed pseudo-randomly every 10 s such that over the two functional runs each speed was cued twice. The actual speed the subject performed the task was self-determined. The number zero was presented to cue a rest epoch.

Each subject's velocity time-series collected during the two functional runs was concatenated, as was the BOLD time-series. The average speed of right D2 movement during each TR (1.5 s) of functional imaging was determined from the MEMS sensor data. A general linear model was applied to detect cortical areas with a BOLD activation response that was linearly related to the speed of D2 movement after accounting for the activation response due to movement. Specifically, the general linear model included a baseline linear drift term, motion-correction parameters, and two stimulus input functions. One stimulus input function was a boxcar function that coded categorically (per TR) for movement and rest. The other stimulus input function was the speed (per TR) time-series. Prior to model fitting, both stimulus input functions were convolved with a gamma variate function (Cohen, 1997). The resultant statistical activation map of interest reflected the linear contribution of finger movement speed to the BOLD activation response. This statistical activation map was corrected to a false discovery rate of 1% and a minimum cluster surface area of 200 mm^2. The corrected statistical activation maps from the two subjects were intersected to determine the common cortical areas exhibiting speed-dependent activation.

Experiment 7

We examined fMRI activation in relationship to on-line motor performance in a chronic stroke patient (male, age 47 years). The stroke in this patient was located in the left hemisphere, and spared the hand region of the primary sensorimotor cortex. The patient was positioned in the scanner with the transmitter/receiver head coil and MEMS sensors on the fingers. Functional images were collected (number of acquisitions/slice = 165) while the patient was performing the five-digit motor task. BOLD images and finger motion data were collected during right and left hand performance in separate functional runs.

The patient's hemodynamic response to finger motion was estimated using a general linear model with inclusion of a baseline linear drift term, motion-correction parameters, and a canonical stimulus input function that was a gamma function (delta = 2.25 s, tau = 1.25 s) convolved with a boxcar function. The cortical surface clusters contiguous with the vertex of maximum significance in the PRG and POG of the hand region within the sensorimotor cortex were identified during right and left hand motor task performance. The time-courses of the BOLD activation response across vertices of the PRG and POG clusters were extracted, from which the mean magnitude of the activation response during the first-period (6–13.5 s after movement onset) and second-period (16.5–24 s after movement onset) of each movement epoch was computed. The sensor data were analyzed to quantify gross (duration, frequency) and finer (amplitude, velocity, acceleration, jerk) characteristics of the patient's finger movement during fMRI. These movement characteristics were computed for the first- and second-periods of the movement epochs for each digit, and averaged over the five digits of a hand. Separate two-way, repeated measures analysis of variance (ANOVA) with one within-subjects factor (moving hand) and one between-subjects factor (movement period) was used to test for main and interaction effects on the BOLD activation response in the regions-of-interest and movement kinematics. Alpha was set to 0.05 for these analyses.

Results and discussion

We built an MEMS-based device that measures the angular velocity of one segment of each of the 10 fingers while a subject performs a motor task during fMRI. The MEMS sensor's small size (7 mm × 7 mm × 3 mm), low weight (<0.5 g), and large dynamic measurement range (±300°/s) make it well suited for fMRI motor studies. The device was built at relatively low cost, and could be replicated with relative ease given that the component parts are commercially available. The sensitivity of the sensors could be adjusted from that used here. We chose to

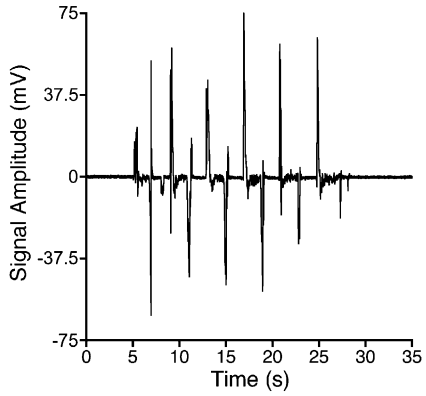

Fig. 3. Representative raw velocity time-series of finger motion acquired during fMRI using the MEMS-based device. The subject was performing repetitive flexion and extension of the five digits of the right hand.

increase the dynamic measurement range of the sensors from the default value of ±150°/s to ±300°/s to better accommodate the range of finger motion velocities we expect our subjects, often stroke patients, will be performing in future fMRI motor studies. However, even with this extended measurement range, there were occasions (approximately 0.1 s in duration) when finger velocity during the motor tasks performed in this series of experiments exceeded 300°/s. Further desensitization of the sensors, which is possible up to ±600°/s, would have eliminated this loss of velocity data.

For the experiments described in the current study, we positioned an MEMS sensor on the proximal segment of each of 10 fingers such that flexion and extension about each metacarpophalangeal joint were detected. Given this positioning, our velocity measurements did not provide complete velocity profiles of the multi-joint movements performed by our subjects. However, there are strong synergies among the joints of a single finger during hand movements performed by normal adults (Grinyagin et al., 2005; Santello et al., 1998), suggesting that our measurements did capture a major component of the performed movement. The experimental needs of future studies might prompt positioning the MEMS sensors differently than applied here. Further, the size and weight of the sensors would allow mounting multiple sensors on a single finger.

Characterizing the MEMS sensor signal (Experiment 1)

Fig. 3 shows a representative raw velocity time-series (i.e., in volts) of finger motion acquired during fMRI using the MEMS-based device when a subject performed the five-digit motor task with the right hand (repetitive flexion and extension of the five digits). Across the five MEMS sensors of the right-hand, there were small differences in the baseline noise range (5.19 ± 2.39 mV) and signal range (198.69 ± 12.21 mV) during this fMRI run. These differences in the baseline noise and signal range were likely due to tolerances of the MEMS sensors (Geen et al., 2002) and its application circuit (Fig. 1). Given these differences, the SNR also varied slightly across the five digit sensors (range: 27.10–34.36 dB). Even with consideration given to the sensor with the lowest SNR, we were clearly able to detect velocity of all five digits during motor task performance. Over the duration of the fMRI run, there were negligible changes in the average baseline noise amplitude at the first as compared to the last rest epoch across the digit sensors (difference = 0.11 ± 0.30 mV). Further, comparing sensor measurements at this fMRI session and another fMRI session conducted 2 weeks later with a different subject, there were negligible changes in the baseline noise range (0.27 ± 1.91 mV), signal range (1.08 ± 13.44 mV), and SNR (ranges: from 27.10–34.36 dB to 29.44–33.48 dB) across the five digit sensors. These data indicate that the MEMS sensors showed non-significant differences in the range of baseline noise, signal, and SNR across the digits and over time.

Effect of MRI on the MEMS sensor signal (Experiments 2 and 3)

Experiments 2 and 3 tested the effect of the static magnetic field and RF fields on the MEMS sensor signal during MRI.

Experiment 2 tested whether signal from the MEMS sensors was corrupted when finger movements were performed at high static magnetic field (3 T) as compared to low static magnetic field (44 G). Determination of the correlation function between the two movement velocity time-series returned an r value of 0.83 with an associated P value of <0.001, indicating a highly significant correlation between the two time-series (Fig. 4). We speculate that this r value was not even closer to 1.0 because the finger movement was performed by a human, which added uncontrolled variability to the finger motion data. Nonetheless, these data suggest that high static magnetic field strength did not contaminate the MEMS sensor signal during finger movement.

Experiment 3, which tested the effect of increasing RF power on the MEMS sensor signal, revealed that the SNR of the sensor signal was 30.7 dB with use of the transmitter/receiver head coil, whereas it was 24.2 dB with use of the transmitter body coil in conjunction with the eight-channel receiver head coil. This loss in SNR, however, did not interfere with the ability to accurately record finger motion at velocities typically occurring during fMRI motor studies (Fig. 5).

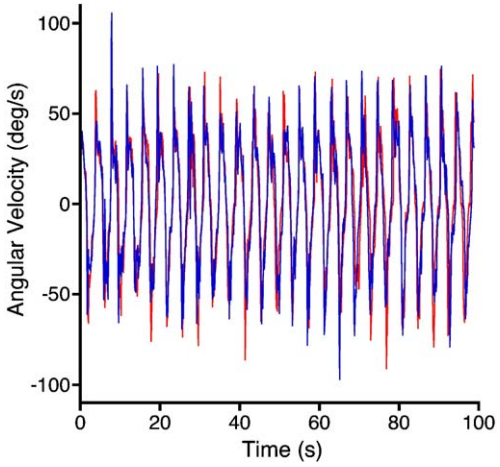

Fig. 4. Angular velocity time-series from the MEMS-based device during movement epochs performed at high (3 T, blue) and low (44 G, red) static magnetic field strength. There was a significant correlation between the two time-series (r = 0.83, P < 0.001), suggesting that the high static magnetic field did not contaminate the MEMS sensor signal during finger movement. The motor task was repetitive flexion and extension of the five digits of the right hand. The time-series of a representative digit (middle finger of right hand) under the two conditions are shown.

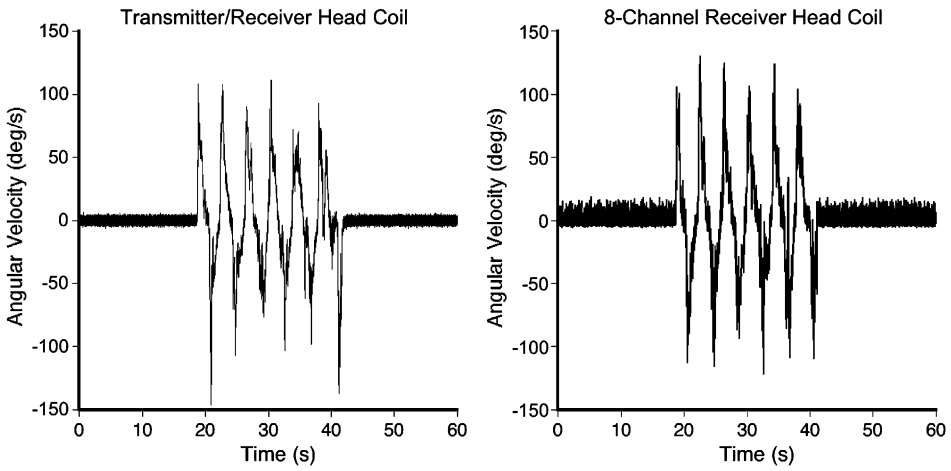

Fig. 5. Angular velocity time-series of finger movement collected during fMRI with use of a transmitter/receiver head coil as compared to a body coil in conjunction with an eight-channel receiver head coil. The fMRI motor task was repetitive flexion and extension of the five digits of the right hand. Shown are time-series of a representative digit (middle finger of right hand) during a movement epoch bounded by rest epochs under the two conditions. The SNR of the angular velocity time-series was decreased with use of the eight-channel receiver head coil (24.2 dB) as compared to the transmitter/receiver head coil (30.7 dB), though this loss did not interfere with the ability to detect velocity of finger motion during fMRI.

Effect of MEMS-based device on the scanning environment and fMR images (Experiments 4 and 5)

We observed no artifacts in the RF noise images collected in the presence or absence of the MEMS-based device (Experiment 4; data not shown), suggesting that use of the MEMS-based device did not introduce frequency-specific RF noise in the ambient scanning environment. There was an increase in average RF noise across the frequency spectrum with use of the MEMS-based device as compared to its absence (mean in absence = 123.33, presence = 123.48; Fig. 6). This difference in RF noise under the two conditions was statistically significant (mean difference = 0.15, $df = 12{,}748$; $t = 4.27$; $P < 0.0001$; paired, two-tailed Student's t test). The magnitude of the increase in RF noise resulting from use of the MEMS-based device was 0.12% relative to the signal present when the device was absent. This percent increase in RF noise would mean that, for a typical fMRI experiment for which the SNR of T2* images is approximately 30, use of the MEMS-based device would decrease the SNR to 29.96. Therefore, we interpret these findings as suggesting that use of the MEMS-based device during fMRI would negligibly affect image quality.

Experiment 5 tested directly whether use of the MEMS-based device during fMRI produced image artifacts or altered the statistical activation map. We observed no evidence of image artifact in the raw BOLD images when the MEMS-based device was used to record a subject's finger movement during

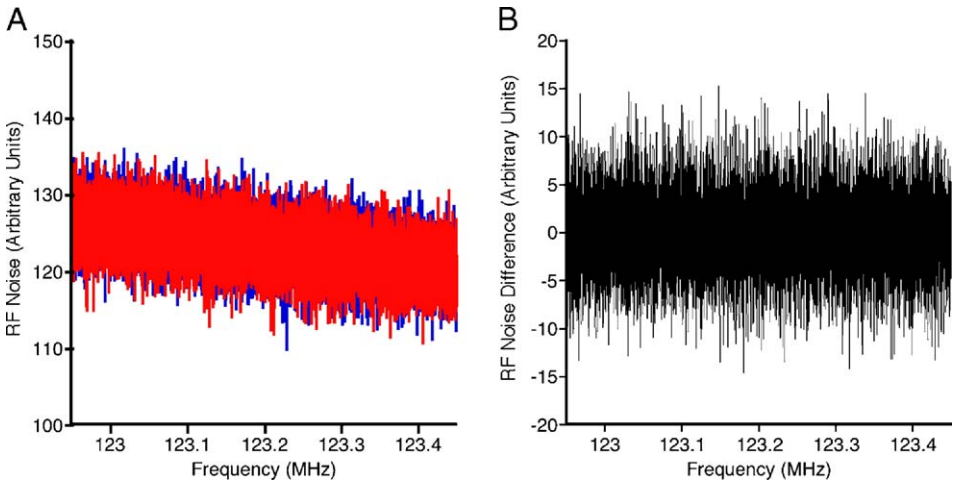

Fig. 6. RF noise imaging conducted during use of the MEMS-based device and in the absence of the device. The motor task was repetitive flexion and extension of the five digits of the right hand. (A) Average RF noise across the frequency spectrum when finger motion data were acquired using the MEMS-based device (blue) and in the absence of the device (red). (B) Difference in RF noise under the two conditions (presence–absence of the device). Across the spectrum, there was a statistically significant difference in the average RF noise under the two conditions ($df = 12{,}748$; $t = 4.27$; $P < 0.0001$; paired, two-tailed Student's t test), with a mean increase of 0.15 in the presence of the sensors. However, this RF noise increase was only 0.12% relative to the signal present in the absence of the sensors, and therefore interpreted as negligible.

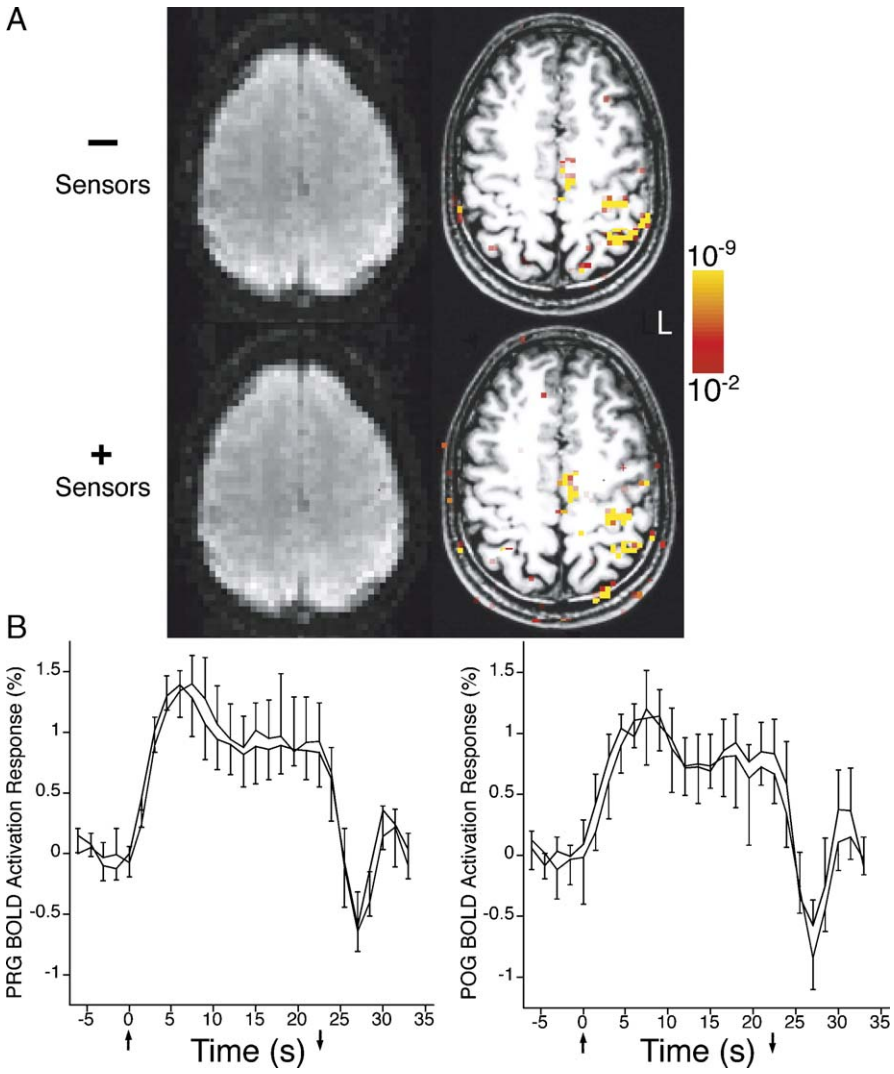

Fig. 7. Functional MRI conducted during use of the MEMS-based device and in the absence of the device. The motor task was repetitive flexion and extension of the index finger of the right hand. (A) Representative axial slice of raw BOLD image data (left column) and the corresponding statistical activation map ($P < 10^{-2}$, corrected) overlaid on T1-weighted image (right column) under the two conditions. L = left hemisphere. No artifacts were observed in the BOLD images acquired with on-line use of the MEMS-based device. Differences in the statistical activation maps under the two conditions were within expected run-to-run variability within a subject. (B) Average BOLD activation response in the PRG and POG acquired in the presence (black) or absence (gray) of the sensors. ↑ = motor task start; ↓ = motor task end.

performance of the motor task (Fig. 7A). Differences between the statistical activation maps computed from the BOLD data collected with and without simultaneous acquisition of finger motion data were within the variability others have observed run-to-run in individual subjects (Tegeler et al., 1999). Across the whole cortical surface, there were no statistically significant differences, using a fixed-effects model and corrected to a false discovery rate of 1%, in the BOLD activation response under the two conditions (data not shown). This result was verified by observing no difference in the time-course of the BOLD activation response under the two conditions in the PRG and POG regions-of-interest (Fig. 7B). Further, the location and spatial extent of the activation response in the PRG and POG were not different under the two conditions (Table 1). Comparable results were found in both subjects' data. These findings strongly indicate that use of the MEMS-based device during fMRI did not interfere with the quality or accuracy of the functional images. Further, the lack of difference in the POG activation response under the two conditions provides evidence that use of the MEMS sensors did not introduce additional somatosensory stimulation during performance of the fMRI motor task.

Table 1
Functional MRI activation in the presence and absence of the MEMS-based device

Region-of-interest	Sensors (±)	Vertex of maximum significance		Cluster size (mm^2)
		Surface vertex number	Talaraich coordinates	
PRG	+	66,026	−37, −7, 62	299
	−	66,026	−37, −7, 62	295
POG	+	58,331	−42, −16, 57	44
	−	58,330	−41, −17, 57	49

Application of the MEMS-based device in fMRI motor studies (Experiments 6 and 7)

Experiment 6 utilized the MEMS-based device to examine speed-dependent brain activation. The range of speed detected by the MEMS sensors during D2 movement was 76 to 497°/s (mean of peak speed over 10-s cued periods), which corresponded to a frequency range of 0.30 to 4.74 Hz. The MEMS sensors maintained sensitivity across a large range of finger movement speed and frequency, suggesting that the MEMS-based device will have broad usefulness in fMRI motor studies.

Analysis of the BOLD data from Experiment 6 revealed that the activation response in the hand region of the primary sensorimotor cortex and, to a lesser extent, the secondary somatosensory cortex within the hemisphere contralateral to moving finger was significantly, positively correlated with the speed of D2 movement (Fig. 8A). Fig. 8B shows exemplar BOLD activation responses in the hand region of the primary sensorimotor cortex that paralleled D2 movement speed. The finding of speed-dependent BOLD activation in the contralateral primary sensorimotor cortex is consistent with previous neuroimaging studies that demonstrated a positive linear relationship between primary sensorimotor cortex activation and the frequency of finger movement in humans (Blinkenberg et al., 1996; Jancke et al., 1998; Kastrup et al., 2002; Rao et al., 1996; Riecker et al., 2003; Schlaug et al., 1996). The linear dependence of the BOLD activation response on movement speed in the secondary somatosensory cortex may have been due to stimulation of deep somatosensory receptors (e.g., joint receptors) during finger motion, as others have shown that activation in this area is linearly increased in response to increasing the frequency of vibrotactile stimulation (Francis et al., 2000; Tanosaki et al., 2003). Prior neuroimaging studies relied on the cued frequency rather than actual motor performance for statistical analysis of frequency-dependent activation. The novelty of our result is that it is based on continuous on-line motor performance during fMRI. The ability of the MEMS-based device to detect continuous finger motion during fMRI is expected to be particularly useful in studies with patients who often exhibit kinematic differences between cued and actual motor performance.

Experiment 7 applied the MEMS-based device to examine fMRI activation in relation to on-line motor performance in a stroke patient. Fig. 9A shows the average time-course of the BOLD activation response in the PRG and POG during motor task performance by the affected and unaffected hands of the patient. Separate two-way, repeated measures ANOVA detected a significant main effect of hand on the activation response in the PRG ($F(1,8) = 7.5$, $P < 0.05$) and POG ($F(1,8) = 32.4$, $P < 0.001$). Furthermore, there was a significant interaction between hand and period in the PRG ($F(1,8) = 8.6$, $P < 0.05$) and the POG ($F(1,8) = 10.9$, $P < 0.05$). These results indicate a time-dependency to the activation response in the PRG and POG during movement of the stroke-affected hand, as compared to the unaffected hand. Fig. 9B shows characteristics of movement of an unaffected and affected finger of the patient, computed from the velocity time-series acquired during fMRI. Separate two-way, repeated measures ANOVA for each movement characteristic revealed significant main effects of hand on fine (i.e., amplitude, velocity, acceleration, jerk magnitudes), but not gross (i.e., duration, frequency), kinematics of motor performance (Table 2). The kinematics of stroke-affected hand movement did not change significantly over time, unlike the associated BOLD activation response. Previous studies in normal humans have demonstrated that the magnitude of the hemodynamic response in the primary sensorimotor cortex is roughly linearly related to several characteristics of finger movement (e.g., rate, amplitude, force) (Blinkenberg et al., 1996; Cramer et al., 2002; Jancke et al., 1998; Kastrup et al., 2002; Riecker et al., 2003; Schlaug et al., 1996; Waldvogel et al., 1999). The mechanism underlying the time-dependent increase in the BOLD activation response in the PRG and POG associated with the affected hand of this stroke patient without a corresponding change in movement kinematics is unknown. It is possible that motor recovery in this patient involved brain reorganization that introduced non-linearities between movement kinematics and primary sensorimotor cortex activity. This

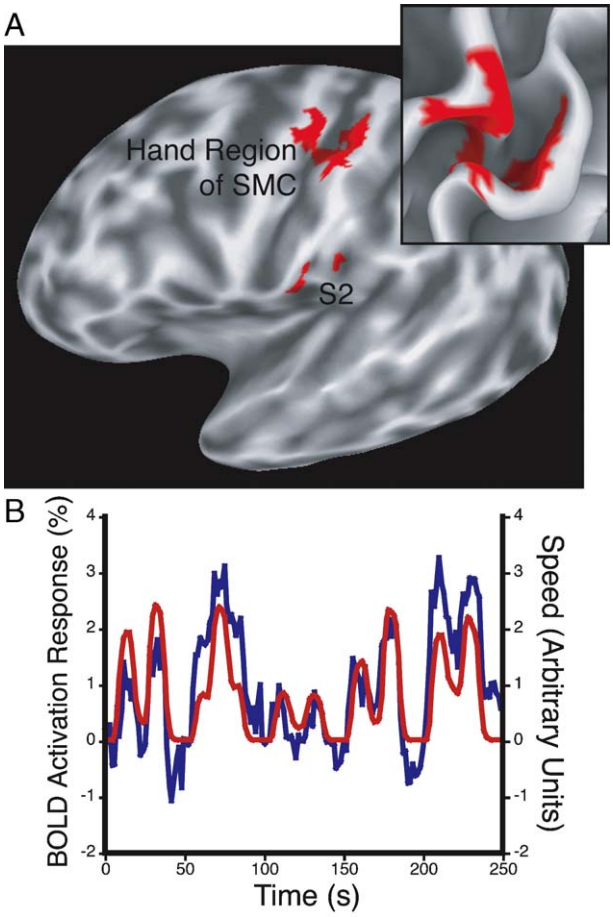

Fig. 8. Speed-dependent BOLD activation response. The motor task was right index finger flexion and extension at variable rates. (A) Cortical areas that exhibited a significant ($P < 10^{-2}$, corrected) linear increase in the activation response with increased movement speed. Results are displayed on an inflated cortical surface model of the left hemisphere. SMC = primary sensorimotor cortex; S2 = secondary somatosensory cortex. Inset displays the hand region of the SMC on the folded, white matter surface model. (B) Representative time-series of finger movement speed (blue) and BOLD activation response (red) averaged across the speed-dependent region of the SMC. The speed time-series displayed (and used in statistical analysis) is the convolution of the speed time-series acquired on-line and a gamma variate function.

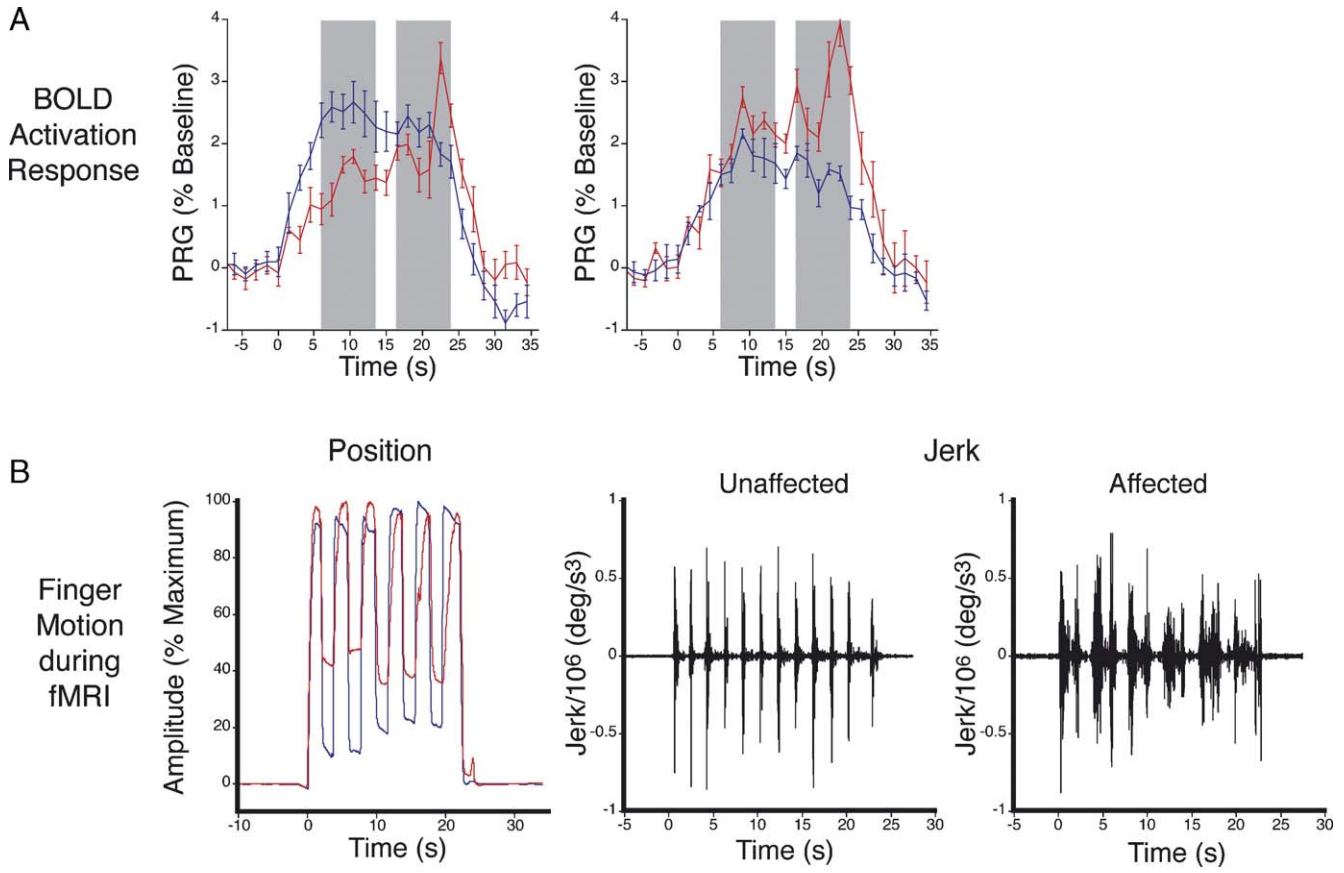

Fig. 9. BOLD activation response and on-line finger movement in a stroke patient. The motor task was repetitive, unilateral flexion and extension of the five digits. Hand movement was cued to start and stop at 0 and 22.5 s, respectively. (A) Time-course of the average BOLD activation response in the PRG and POG during affected (red) and unaffected (blue) hand motor task performance. Values are mean ± standard error. Gray bars indicate first- and second-periods of the hemodynamic response to movement. Separate two-way, repeated measures ANOVA detected a significant main effect of hand on the activation response in the PRG ($F(1,8) = 7.5$, $P < 0.05$) and POG ($F(1,8) = 32.4$, $P < 0.001$), and a significant interaction between hand and period in the PRG ($F(1,8) = 8.6$, $P < 0.05$) and the POG ($F(1,8) = 10.9$, $P < 0.05$). (B) Position time-series of a representative digit (middle finger) of the affected (red) and unaffected (blue) hand, and jerk time-series of the same digit during a representative movement epoch. Separate two-way, repeated measures ANOVA detected a significant main effect of hand on peak amplitude ($F(1,8) = 52.8$, $P < 0.0001$) and jerk magnitude ($F(1,8) = 32.8$, $P < 0.001$).

preliminary result suggests that conducting an fMRI motor study that utilized the MEMS-based device to measure on-line finger motion in patients with a range of residual motor impairments would be valuable to characterize the relationship between movement kinematics and brain activation after stroke.

Table 2
Characteristics of finger motion during fMRI in a stroke patient

	Moving hand	
	Unaffected	Affected
Finger motion characteristic		
Duration (s)	20.4 ± 0.8	20.9 ± 0.5
Frequency (Hz)	0.25 ± 0.00	0.25 ± 0.00
Peak amplitude (% max)	89.0 ± 4.0	70.3 ± 6.7‡
Velocity magnitude (°/s)	50.1 ± 2.2	45.2 ± 3.2†
Acceleration magnitude (°/s^2)	715 ± 31	1097 ± 137‡
Jerk magnitude (°/s^3)	44,622 ± 3320	62,874 ± 8354†

†$P < 0.001$, ‡$P < 0.0001$ versus unaffected hand, main effect, two-way repeated measures ANOVA. Values are mean ± SD.

Conclusions

We built an MRI-compatible device using MEMS sensors that measures the angular velocity of a single segment of each of the 10 fingers. The series of experiments described here demonstrate that the SNR of the MEMS sensor signal allows for clear detection of finger velocities during motor tasks typically performed during fMRI. The sensitivity of the MEMS sensors during fMRI was quite stable over time. Further, we showed that the scanning environment did not interfere with the ability to accurately record finger motion using the MEMS-based device, and, reciprocally, its use does not cause fMR image artifacts. We provided two examples of the utility of the MEMS sensors in fMRI motor studies. The angular velocity measurements were used to compute several kinematic features of the finger movement that occurred on-line during fMRI motor studies, including frequency, position, speed, acceleration, and jerk.

We envision that the MEMS-based device will be useful in future fMRI motor studies to achieve a more detailed understanding of the relationship between movement kinematics and activation in the healthy and injured brain. For example, the

MEMS-based device could make possible real-time monitoring and feedback of movement kinematics in virtual environments during fMRI. Such an application could provide greater insight into the brain mechanisms controlling motor learning in patients with motor dysfunction. The device could also permit evaluating the efficacy of therapeutic interventions, for example physical rehabilitation in stroke patients, using a combination of fMRI and on-line kinematic data.

Acknowledgments

This work was supported by a grant to J.D.S. from the NIH-NCMRR (K23-HD044425), to G.B. from the NIH-NIBIB (RO1-EB002459-01), the NCRR (P41-RR14075), and the MIND Institute. We thank Andreas Potthast, Dipl.-Ing. and Franz Hebrank, Ph.D. for valuable discussions about RF noise imaging, and Dr. Hebrank for providing useful feedback on a draft of the manuscript.

References

Blinkenberg, M., Bonde, C., Holm, S., Svarer, C., Anderson, J., Paulson, O.B., Law, I., 1996. Rate dependence of regional cerebral activation during performance of a repetitive motor task: a PET study. J. Cereb. Blood Flow Metab. 16, 794–803.

Carey, J.R., Kimberley, T.J., Lewis, S.M., Auerbach, E.J., Dorsey, L., Rundquist, P., Urgurbil, K., 2002. Analysis of fMRI and finger tracking training in subjects with chronic stroke. Brain 125, 773–788.

Cohen, M.S., 1997. Parametric analysis of fMRI data using linear systems methods. NeuroImage 6, 93–103.

Cramer, S.C., Weisskoff, R.M., Schaechter, J.D., Nelles, G., Foley, M., Finklestein, S.P., Rosen, B.R., 2002. Motor cortex activation is related to force of squeezing. Hum. Brain Mapp. 16, 197–205.

Dale, A.M., Buckner, R.L., 1999. Selective averaging of rapidly presented individual trials using fMRI. Hum. Brain Mapp. 5, 329–340.

Dale, A., Fischl, B., Sereno, M., 1999. Cortical surface-based analysis: I. Segmentation and surface reconstruction. NeuroImage 9, 179–194.

Ehrsson, H.H., Fagergren, E., Forssberg, H., 2001. Differential fronto-parietal activation depending on force used in a precision grip task: an fMRI study. J. Neurophysiol. 85, 2613–2623.

Francis, S.T., Kelly, E.F., Bowtell, R., Dunseath, W.J., Folger, S.E., McGlone, F., 2000. fMRI of the responses to vibratory stimulation of digit tips. NeuroImage 11, 188–202.

Geen, J., Sherman, S., Chang, J., Lewis, S., 2002. Single-chip surface micromachined integrated gyroscope with 50 deg/h Allan deviation. IEEE J. Solid-State Circuits 37, 1860–1866.

Genovese, C.R., Lazar, N.A., Nichols, T., 2002. Thresholding of statistical maps in functional neuroimaging using the false discovery rate. NeuroImage 15, 870–878.

Grinyagin, I.V., Biryukova, E.V., Maier, M.A., 2005. Kinematic and dynamic synergies of human precision-grip movements. J. Neurophysiol. 94, 2284–2294.

Jancke, L., Specht, K., Mirzazade, S., Loose, R., Himmelbach, M., Lutz, K., Shah, N.J., 1998. A parametric analysis of the 'rate effect' in the sensorimotor cortex: a functional magnetic resonance imaging analysis in human subjects. Neurosci. Lett. 252, 37–40.

Kastrup, A., Kruger, G., Neumann-Haefelin, T., Glover, G.H., Moseley, M.E., 2002. Changes of cerebral blood flow, oxygenation, and oxidative metabolism during graded motor activation. NeuroImage 15, 74–82.

Liu, J.Z., Dai, T.H., Elster, T.H., Sahgal, V., Brown, R.W., Yue, G.H., 2000. Simultaneous measurement of human joint force, surface electromyograms, and functional MRI-measured brain activation. J. Neurosci. Methods 101, 49–57.

Moore, C.I., Stern, C.E., Corkin, S., Fischl, B., Gray, A.C., Rosen, B.R., Dale, A.M., 2000. Segregation of somatosensory activation in the human rolandic cortex using fMRI. J. Neurophysiol. 84, 558–569.

Morgen, K., Kadom, N., Sawaki, L., Tessitore, A., Ohayon, J., Frank, J., McFarland, H., Martin, R., Cohen, L.G., 2004. Kinematic specificity of cortical reorganization associated with motor training. NeuroImage 21, 1182–1187.

Rao, S.M., Bandettini, P.A., Binder, J.R., Bobholz, J.A., Hammeke, T.A., Stein, E.A., Hyde, J.S., 1996. Relationship between finger movement rate and functional magnetic resonance signal change in human primary motor cortex. J. Cereb. Blood Flow Metab. 16, 1250–1254.

Reilly, J., 1998. Applied Bioelectricity. Springer-Verlag, New York.

Riecker, A., Wildgruber, D., Mathiak, K., Grodd, W., Ackermann, H., 2003. Parametric analysis of rate-dependent hemodynamic response functions of cortical and subcortical brain structures during auditorily cued finger tapping: a fMRI study. NeuroImage 18, 731–739.

Rowe, J.B., Frackowiak, R.S., 1999. The impact of brain imaging technology on our understanding of motor function and dysfunction. Curr. Opin. Neurobiol. 9, 728–734.

Santello, M., Flanders, M., Soechting, J.F., 1998. Postural hand synergies for tool use. J. Neurosci. 18, 10105–10115.

Schlaug, G., Sanes, J.N., Thangaraj, V., Darby, D.G., Jancke, L., Edelman, R.R., Warach, S., 1996. Cerebral activation covaries with movement rate. NeuroReport 7, 879–883.

Shellock, F.G., 2002. Magnetic resonance safety update 2002: implants and devices. J. Magn. Reson. Imaging 16, 485–496.

Tanosaki, M., Sato, C., Shimada, M., Iguchi, Y., Hoshi, Y., 2003. Effect of stimulus frequency on human cerebral hemodynamic responses to electric median nerve stimulation: a near-infrared spectroscopic study. Neurosci. Lett. 352, 1–4.

Tegeler, C., Strother, S.C., Anderson, J.R., Kim, S.G., 1999. Reproducibility of BOLD-based functional MRI obtained at 4 T. Hum. Brain Mapp. 7, 267–283.

Thesen, A., Heid, O., Mueller, E., Schad, L.R., 2000. Prospective acquisition correction for head motion with image-based tracking for real-time fMRI. Magn. Reson. Med. 44, 457–465.

Waldvogel, D., van Gelderen, P., Kenji, I., Hallett, M., 1999. The effect of movement amplitude on activation in functional magnetic resonance imaging studies. J. Cereb. Blood Flow Metab. 19, 1209–1212.

Wexler, B.E., Fulbright, R.K., Lacadie, C.M., Skuldarski, P., Kelz, M.B., Constable, T., Gore, J.C., 1997. An fMRI study of the human cortical motor system response in increasing functional demands. Magn. Reson. Imaging 15, 385–396.